CLIMATOLOGY

The emerging human fingerprint on global extreme fire weather

Marco Turco[1]*†, Alberto Moreno[1]†, Ginés Garnés-Morales[1], Miguel Ángel Torres-Vázquez[2], Francesca Di Giuseppe[3], Joaquín Bedia[4], Sixto Herrera[4], Antonello Provenzale[5,6], John T. Abatzoglou[7]

Extreme fire weather (hot, dry, and windy conditions) has intensified globally, yet formally attributing this trend to anthropogenic climate change remains challenging. Here, we analyze global trends in extreme fire weather days (FWI95d, annual count of days with Fire Weather Index above the 95th percentile) over 1980–2023, using climate model ensembles, observational data, and fingerprint detection techniques. We find that the observed increase in extreme fire weather bears a clear externally forced signal, detectable at 99% confidence above natural variability and attributable to human-induced climate change. This emerging human-induced fingerprint on extreme fire weather highlights a benchmark for climate science and underscores the urgency of integrating these insights into wildfire risk management and adaptation strategies.

INTRODUCTION

Wildland fires occur when an ignition—either natural or human—concurrently interacts with continuous fuels under suitable weather conditions to sustain fire spread (*1*). Fire weather—defined by a combination of hot, dry, and windy conditions—influences ignition potential, fuel flammability, and fire spread (*2*, *3*).

Given the sensitivity of fire activity to fire weather, understanding how climate change and variability affect these conditions is essential for gauging the required management efforts in an increasingly flammable landscape, determining where and when such efforts are most needed, assessing their feasibility, and ultimately mitigating escalating wildfire hazard as part of effective risk assessment and adaptation strategies. Extreme fire weather conditions are closely linked to severe wildfire events (*4*), which have increased markedly in both intensity and frequency in recent years (*5*). For instance, Jones *et al.* (*6*) found that in one extratropical forest region, annual emissions tripled due to increasingly fire-favorable weather, further amplified by rising forest cover and productivity, contributing to a 60% increase in global carbon emissions from forest fires during 2001–2023.

In recent decades, extreme fire weather days have increased markedly in frequency, duration, and geographic extent (*7*–*11*). Although anthropogenic climate change is widely believed to have amplified these hazardous conditions [see, e.g., (*12*)], formally attributing the observed changes to human influence remains challenging because natural climate variability substantially affects the meteorological drivers of the Fire Weather Index (FWI) (*13*). Natural variability plays a substantial role in shaping fire weather patterns across different regions and timescales [see, e.g., (*14*)]. Various modes of climate variability—such as the El Niño–Southern Oscillation (ENSO), Atlantic Multidecadal Oscillation, North Atlantic Oscillation (NAO), and Pacific Decadal Oscillation (PDO)—influence regional fire weather conditions (*15*–*18*) by modulating key factors including temperature, precipitation, wind speed, and relative humidity (RH) (*19*–*22*). These natural fluctuations can obscure with the anthropogenic signal, complicating efforts to quantitatively determine the influence of human activities on fire weather patterns. Consequently, a formal attribution effort is crucial for establishing how much anthropogenic climate change and natural variability, respectively, contribute to the observed increases in FWI across different regions and timescales.

In this study, we address this gap by providing a global attribution of observed changes in the FWI, distinguishing internal variability from a response to external forcing in the FWI changes. Using climate models (*23*, *24*), observation-based reanalysis datasets (*25*–*27*), and robust fingerprint detection methods (*28*, *29*), we disentangle the external signal from natural variability in fire weather trends. Fingerprint detection leverages pattern information in observed changes to distinguish external influences from naturally occurring climate fluctuations.

By extending attribution techniques, traditionally applied to temperature [see, e.g., (*29*–*31*)], and hydroclimatic variables [see, e.g., (*32*, *33*)], to fire weather metrics, we present compelling evidence of a clear link between external influences and the escalation of dangerous fire weather. As discussed below, such external influences are most likely associated with human-induced climate change. These findings underscore the urgency of integrating this knowledge into global fire management strategies as well as climate adaptation frameworks.

RESULTS

Trend assessment

We begin by examining whether the HIST+245 simulations (historical simulations concatenated with SSP2-4.5 simulations) capture the main characteristics of observed FWI95d trend patterns. Demonstrating skill in reproducing these patterns strengthens confidence in the subsequent fingerprint analysis. Overall, the three datasets—ERA5, JRA55, and the Coupled Model Intercomparison Project Phase 6 (CMIP6) ensemble mean (ENSMEAN)—show substantial agreement on areas with rising extreme fire weather, although, as we will

[1]Department of Physics, Regional Campus of International Excellence (CEIR) Campus Mare Nostrum, University of Murcia, Murcia, Spain. [2]Universidad de Alcalá, Environmental Remote Sensing Research Group, Department of Geology, Geography and the Environment, Calle Colegios 2, Alcalá de Henares 28801, Spain. [3]European Center for Medium-range Weather Forecast (ECMWF), Reading, UK. [4]Department of Applied Mathematics and Computing Science, Universidad de Cantabria, Santander, Spain. [5]Institute of Geosciences and Earth Resources, National Research Council, Torino, Italy. [6]CIMA Research Foundation, Via Armando Magliotto, 17100 Savona, Italy. [7]School of Engineering, University of California, Merced, USA.
*Corresponding author. Email: marco.turco@um.es
†These authors contributed equally to this work.

see below, some local discrepancies exist (Fig. 1). This is supported by statistically significant, area-weighted spatially averaged Pearson correlations: ERA5 versus JRA55: 0.536 ($P < 0.001$), ERA5 versus ENSMEAN: 0.336 ($P < 0.001$), JRA55 versus ENSMEAN: 0.231 ($P < 0.001$).

ERA5 exhibits near-global increases in FWI95d, with notable exceptions over India and parts of Southeast Asia where trends are negative. Both JRA55 and the CMIP6 ensemble mean broadly reproduce this pattern but with weaker slopes overall and more extensive areas of weak or negative trends (Fig. 1). Consistent with previous studies [e.g., (*2*, *7*, *9*)], both reanalysis products and the CMIP6 ensemble mean highlight pronounced increases in the western United States—where recent severe wildfires, including those in the Los Angeles area in January 2025, are consistent with the escalating fire risk—along with southern and central Europe (*34*), Brazil, and parts of central and southern Africa. In contrast, a pronounced negative trend over India appears consistently in both reanalyses and the simulations. Linear trends were computed using ordinary least squares regression, in line with standard practice in detection and attribution studies [e.g., (*29*)]. As a robustness check, we also tested the Theil-Sen estimator and found negligible differences in the spatial patterns and magnitudes of the trends (fig. S1).

Despite broad agreement on large-scale trends, regional variations become apparent. In central-southern Africa, for example, notable discrepancies emerge between the JRA55 and ERA5 datasets in terms of both trend magnitude and direction. This divergence is attributable to the well-known challenges that reanalyses face in accurately representing tropical climates (*35*, *36*), where high variability in convective rainfall and limited observational data contribute to these differences (*37*). These issues highlight the importance of carefully evaluating and comparing multiple datasets when examining FWI trends, particularly in tropical regions where individual reanalyses may differ markedly.

A similar contrast emerges when comparing the ensemble mean with individual reanalysis datasets. The ensemble mean, by averaging multiple realizations, smooths out internal variability and emphasizes the externally forced climate signals. In contrast, observations capture only a single realization of internal variability overlaid on the externally forced trend, making observed patterns inherently noisier. Individual climate model simulations, unlike the ensemble mean, can replicate similar levels of variability (see figs. S3 and S4). Despite these nuances, the consistent large-scale fire weather trends across datasets justify proceeding with the fingerprint analysis presented in the following sections.

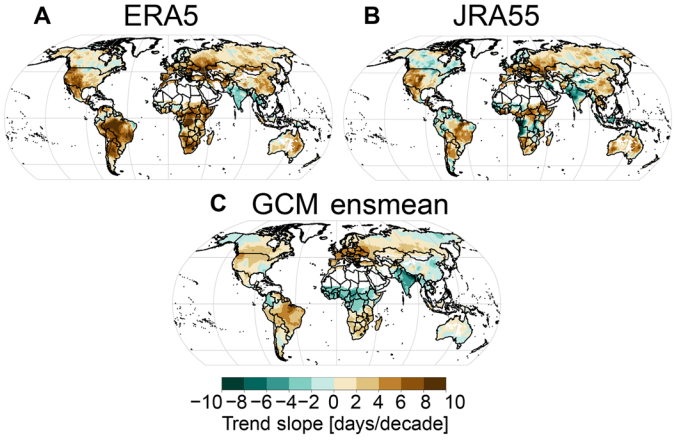

Fig. 1. Global trends in extreme fire weather conditions (FWI95d). Trends in the total annual number of days exceeding the 95th percentile of the FWI (FWI95d) from 1980 to 2023. The panels display results from different sources: (**A**) ERA5 reanalysis, (**B**) JRA55 reanalysis, and (**C**) a multimodel ensemble mean derived from climate models incorporating external forcing. Regions with infrequent fire activity have been excluded.

Fingerprint analysis

Following (*28*, *29*), we test whether model-derived fingerprints of external forcing can be statistically identified in observed FWI95d data. The basic idea is to detect externally forced changes by reducing the influence of internal climate variability. This approach assumes the internal climatic variability (i) to be uncorrelated across multiple model realizations and (ii) to be stationary, with statistical properties constant over time. In such conditions, the expected response to external forcing is estimated by averaging over many forced simulations, and the fingerprint is then defined as the leading empirical orthogonal function (EOF) of the FWI95d multimodel mean. This approach effectively minimizes the impact of internal variability, allowing the externally forced response to stand out.

Along these lines, we first define the fingerprint as the leading EOF1 of the multimodel mean FWI95d anomalies from CMIP6 HIST+245 simulations over 1980–2023 (Fig. 2A). This fingerprint reflects the dominant spatial pattern of changes, similar to what is shown in Fig. 1, and explains 43% of the total variance, representing the dominant spatial pattern of externally forced changes in extreme fire weather. The principal component time series associated with EOF1 is shown in fig. S2. It displays a clear upward trend over 1980–2023, indicating an increasing amplitude of the dominant fingerprint pattern over time.

To account for internal variability, we also derived a separate EOF1 from 3143 years of concatenated preindustrial control simulations (Fig. 2B), accounting for 5.9% of the total variance. This pattern represents the dominant mode of natural internal climate variability in FWI95d in the absence of external forcing, bearing a strong resemblance to an ENSO-like pattern (see fig. S5). Notably, the second EOF from the CMIP6 HIST+245 simulations closely mirrors the piControl EOF1 (see fig. S6).

The next step is to determine whether the similarity between the HIST+245 fingerprint and the observed FWI95d patterns increases over time and whether this increase is statistically significant relative to random fluctuations driven by internal climate variability. To this end, we compared the HIST+245 fingerprint with the FWI95d patterns derived from (i) reanalysis data and (ii) model control runs, respectively yielding the "signal" and "noise" time series. The ratio of these two ["signal-to-noise" (S/N)] quantifies the detectability of externally forced trends (Fig. 3). We also replaced the reanalysis data with individual HIST+245 model realizations ("model-only" results) to compare how the fingerprint emerges in modeled versus observed datasets.

The reanalyses (ERA5 and JRA55) exhibit a steadily increasing S/N ratio over time, reaching values of approximately 3 to 7, above the 99% confidence detection threshold (≈2.3). Among these, ERA5 shows the strongest and most persistent signal, with JRA55 following a similar trajectory but surpassing the detection threshold only later. The model-only curves (gray lines) display comparable S/N ranges (about 2 to 4), indicating that the strength and time evolution of the fingerprint is similar in models and reanalysis data. ERA5

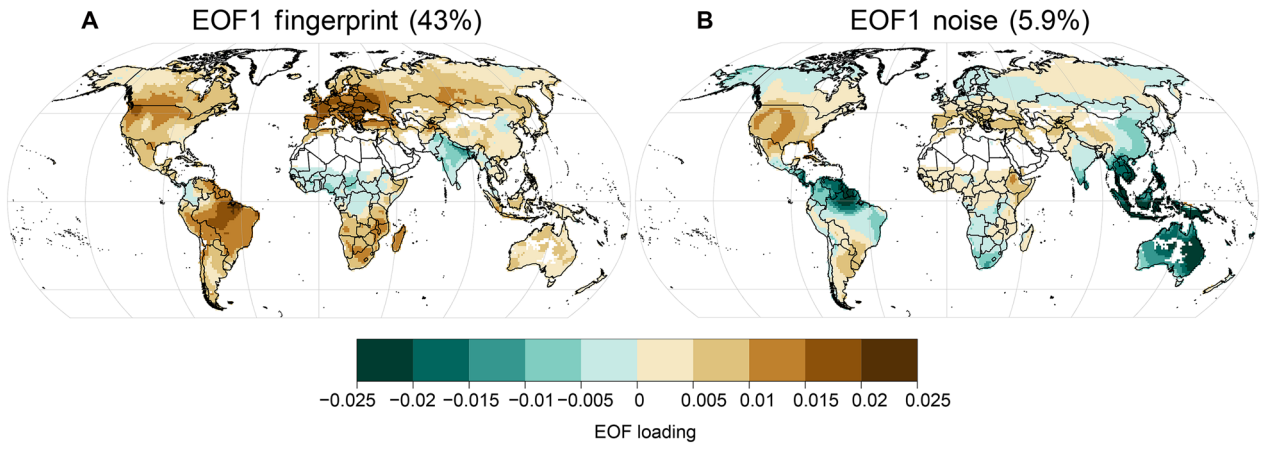

Fig. 2. First EOF1 of FWI95d anomalies. (**A**) Leading EOF1 of the multimodel mean changes in FWI95d anomalies from HIST+245 simulations over 1980–2023, referred to as the "fingerprint." (**B**) Leading EOF1 of concatenated preindustrial control simulations.

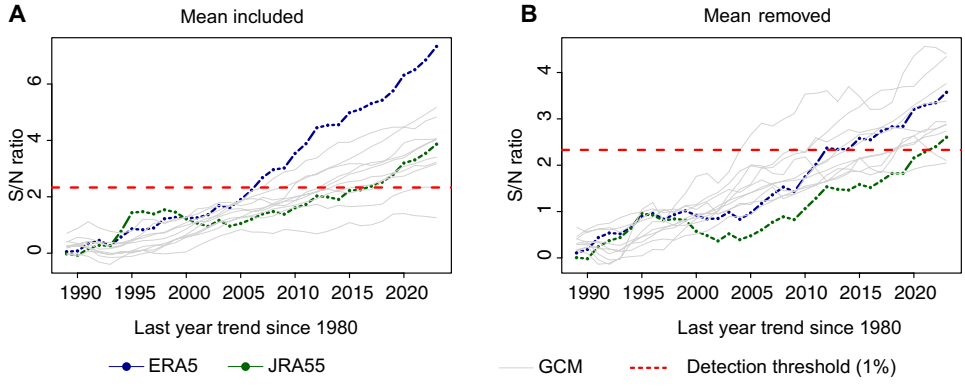

Fig. 3. S/N ratio trends for FWI95d (1980–2023) in reanalyses and GCMs. Temporal evolution of the S/N ratio for trends in the annual number of extreme fire weather days (FWI95d) derived from reanalyses (ERA5 and JRA55) and GCMs under HIST+245 simulations. S/N ratios were calculated by comparing the observed and modeled trends to the internal climate variability. The red dashed line represents the 1% detection threshold, above which the detection of externally forced changes is considered to be statistically robust. (**A**) S/N ratios calculated using the raw FWI95d trend patterns, where each grid point includes the contribution from the global mean (i.e., spatial average ⟨FWI95d(t)⟩ is retained in each year *t*). (**B**) Results for the "mean removed" case, where the global mean FWI95d time series ⟨FWI95d(t)⟩ is subtracted from each grid point/year. Note that the two panels use different vertical scales to enhance readability.

shows higher S/N ratios than any individual global climate model (GCM), particularly after the early 2000s (Fig. 3A). This elevated S/N ratio arises primarily from the relatively strong global mean trends in ERA5 FWI95d (Fig. 1A), which exceed those simulated by most GCMs (figs. S3 and S4). Several factors could explain this discrepancy. First, ERA5 may exhibit systematic biases in certain regions—for example, overly warm, dry, or windy conditions in parts of Africa and the tropics, where observational constraints are weaker and the reanalysis relies more heavily on model outputs (*38*). Second, GCMs might underestimate the magnitude of observed trends in extreme fire weather, potentially due to coarse spatial resolution or incomplete representation of, for instance, land-atmosphere interactions or cloud processes (*39*, *40*). Third, models may not fully capture the observed evolution of large-scale climate variability patterns, such as the PDO (*41*), which has been linked to warming and drying trends in highly fire-prone regions like the western United States (*42*). These factors likely contribute in a combined way, highlighting the complexity of accurately representing regional extremes in both reanalyses and models.

To assess whether detection is driven primarily by changes in the global mean rather than by true spatial pattern similarity, we compute the S/N ratio with and without removing the global mean from the model and observational datasets at each time step. This approach helps identify the spatial pattern of change independent of its overall magnitude. In general, removing the global mean yields slightly lower S/N values. For example, ERA5 barely reaches 3, and JRA55 is similarly reduced. Nevertheless, S/N values remain above the detection threshold, indicating that the detection does not rely solely on global mean trends but also reflects spatial pattern coherence. The model-only results again align well with reanalysis-based S/N, highlighting the consistency of externally forced signals across data sources.

Following (*43*), we also removed regions where approximations of daily FWI—based on mean temperature, RH, wind speed, and precipitation—failed to capture noon-specific trends. Even with these regions excluded, external influence on extreme fire weather trends remains detectable (fig. S7).

Overall, these results show that the fingerprint of external forcing in the increasing extreme fire weather (FWI95d) is both robust

and statistically distinguishable from internal variability. The observed changes cannot be explained solely by natural fluctuations; rather, they reflect the substantial role of external drivers in shaping global fire weather extremes changes.

DISCUSSION

Wildfire activity is closely linked to weather conditions, with compound extremes—such as simultaneous heatwaves, droughts, and strong winds—accelerating fuel drying and fire spread. In recent years, record-breaking wildfire seasons have affected regions including the western United States, the Mediterranean, the Amazon, and Australia (*4*, *9*, *44*). Catastrophic events such as the 2025 and 2020 California wildfires, the 2023 Canadian fire season, and the 2020 Australian Black Summer are consistent with this escalating risk.

Most attribution studies have focused primarily on temperature and precipitation extremes or on linking fire activity—such as burned area and fire typologies—to anthropogenic warming at regional scales (*45*–*47*). These studies generally confirm that human-induced climate change intensified fire weather conditions and increased the likelihood or severity of extreme fire behavior. However, drawing definitive global-scale conclusions remains challenging due to methodological differences and a lack of consistent analyses of multivariate fire weather metrics like the FWI. While fingerprint analyses have been successfully applied to other climate factors, this work represents one of the first attempts to use such an approach for global fire weather.

In this study, we address this gap using FWI-based fingerprint detection methods that integrate multiple datasets—including reanalyses and CMIP6 multimodel simulations—to identify and quantify external influences on the observed changes in fire weather. We use the FWI to assess changes in meteorological conditions conducive to high or extreme synchronous fire danger. Because climate change directly affects fire weather, our method isolates its effects without the confounding influences that affect realized fires (e.g., ignitions, fuel characteristics, and suppression), which are not represented in the FWI formulation. Our findings reveal a distinct external driving signal in the observed escalation of extreme fire weather (FWI95d) worldwide, with key hotspots in western North America, southern and central Europe, Brazil, and parts of Africa. Although the Sixth Assessment Report of the Intergovernmental Panel on Climate Change (IPCC) (*48*) assigned only medium confidence to human-induced increases in fire weather in certain regions, based on the limited literature available at that time, our global-scale analysis provides updated evidence that supports a higher confidence in attributing these trends to external forcing.

In the approach followed here, we cannot directly identify anthropogenic effects; rather, we distinguish the internal climatic variability from external forcing effects. In the absence of any other obvious increasing external influence, the detected external forced change is presumably associated with anthropogenic forcings. One possible problem could emerge if the internal variability had oscillations with long temporal periods, say much longer than the observation window, and all oscillations were in the same phase in the different model runs analyzed here. For example, this could happen if the climatic variability were driven by an increasing or decreasing solar forcing or volcanic activity. However, major volcanic eruptions such as El Chichón (1982) and Pinatubo (1991) produce only short-term, transient cooling signals, and there is no evidence of persistent trends in volcanic or solar activity over the past century that could explain the detected signal [see, e.g., (*29*, *31*)]. Another option would be that all model runs were on the same path to a tipping point or emerging from the same climatic instability. In this case, a slow internal variation could be erroneously ascribed to the action of external forcing. However, it is not clear why the phases of such long-term oscillations should be the same across the ensemble of different model realizations. Under such conditions, we can safely associate the external forcing with the impact of human activities on global climate.

Future studies could further refine our understanding by separating the contributions of different anthropogenic drivers. Anthropogenic forcing includes increases in greenhouse gases (GHGs), aerosol emissions, and land use or land cover changes, all of which may have distinct effects on fire weather conditions. For instance, GHGs tend to raise surface temperatures, thereby enhancing fire weather, while aerosols may locally offset warming or affect humidity and cloud formation. Land use changes can also influence fuel availability and surface energy fluxes. Disentangling these individual contributions could be pursued using single-forcing simulations from the Detection and Attribution Model Intercomparison Project (*24*), such as the hist-GHG (which includes only historical GHG forcing) and hist-aer (which includes only anthropogenic aerosol forcing) experiments, thereby enabling a more detailed attribution of observed fire weather trends.

The strength of our analysis lies in enhancing the S/N ratio. First, by simultaneously considering changes across multiple regions—such as the northwestern United States, southern Europe, Australia, and parts of Africa and Asia—we increase the robustness of the signal, as it is highly unlikely that internal variability alone could produce consistent trends in such geographically and climatologically distinct regions. Second, using spatial patterns allows us to minimize the impact of internal climate variability modes (such as ENSO and NAO), which can induce contrasting FWI changes in different regions at the same time. By incorporating multiple regions with diverse sensitivities to such variability, the fingerprint method averages out these effects, helping to isolate the component of change that is due to external forcing. This rationale aligns with previous detection studies using spatial fingerprints [see, e.g., (*30*)] and reinforces our finding that detection remains robust even when the global mean trend is removed.

Much of the S/N in our analysis arises from the "mean included" case [i.e., when including $\langle \mathrm{FWI95d(t)} \rangle$, the spatially averaged FWI95d for each year], reflecting the broad contribution of global-scale warming. However, we show that detection remains robust even when the global mean is removed. This indicates that the spatial fingerprint contains additional signals beyond simple warming. Regions such as western North America, southern and central Europe, eastern Australia, and parts of South America and Africa exhibit pronounced positive trends in FWI95d. In contrast, India and parts of South Asia show negative trends, a pattern consistent across models and reanalyses. These features can be understood through the physical drivers of fire weather. While FWI generally increases with rising temperature, it is also highly sensitive to RH, which exhibits more complex and regionally heterogeneous trends. For instance, declining dew point temperatures in semiarid regions (e.g., the western US, Brazil, and southern Africa) amplify RH declines, thereby enhancing FWI trends (*7*, *43*). Conversely, regions such as India may experience FWI decreases due to increased atmospheric moisture, potentially related to large-scale circulation changes, aerosol-cloud interactions, or local irrigation practices. While the exact mechanisms remain under investigation, this "warming hole" over India has been discussed in recent literature [see, e.g., (*49*)].

To sum up, these physically interpretable features underscore the added value of spatial fingerprinting. Our positive detection results are unaffected by reanalysis choice (ERA5 or JRA55), by the removal of global mean changes, or by the exclusion of regions where daily approximations distort noon-based FWI estimates.

Of course, climate forcing is only part of the story; human activities also shape fire regimes through ignition practices, land use changes, and suppression efforts (*2*). Nonetheless, our results confirm that external climate forcing, likely associated with anthropogenic GHG emissions, has intensified fire danger by altering key climate variables, suggesting that if fuel availability and ignition patterns remain relatively unchanged, an increase in FWI will likely translate into an increase in fire activity.

From a policy standpoint, these findings underscore the urgent need for targeted adaptation and mitigation strategies. Enhanced wildfire management, expanded early warning systems, and strengthened community resilience can help reduce immediate risks. Our detection of an externally driven signal in FWI95d trends reinforces the importance of sustained mitigation—especially rapid reductions in GHG emissions—to limit the future escalation of fire danger. Such combined efforts aim to achieve a balanced coexistence with fire, acknowledging its ecological role while mitigating the growing threats posed by a warmer, drier climate.

MATERIALS AND METHODS

FWI calculation

The FWI (*13*) is widely used to assess how climate and weather conditions influence wildfire spread once ignited. It combines precipitation, air temperature, RH, and wind speed to estimate fire danger (*27*). Although originally developed for Canadian forests, the FWI is now applied worldwide for both operational and research purposes (*2*, *9*, *27*, *50*, *51*). The FWI has been shown to track both interannual burned area variability and extreme fire events across diverse ecosystems (*4*, *9*, *52*).

Accurate FWI estimates require subdaily meteorological data, but these data are frequently limited by short observation periods, incomplete spatial coverage, and quality issues. Reanalysis datasets, produced by assimilating observations into atmospheric models, offer a continuous and spatially homogeneous alternative (*53*). Still, uncertainties in assimilated data and model limitations can affect FWI estimates (*54*–*56*). Despite these shortcomings, many recent studies use reanalysis products to track historical FWI trends [e.g., (*2*, *6*, *7*, *9*), particularly the Copernicus Emergency Management Service FWI dataset (*27*) based on ERA5 (*25*)].

A further challenge is that the FWI was designed to estimate peak fire danger in the midafternoon (typically around 16:00), using meteorological inputs recorded at local noon, specifically 2-m temperature, 2-m humidity, 24-hour accumulated precipitation, and 10-m wind speed. This timing was chosen because, in boreal regions, weather conditions at local noon have been shown to correlate strongly with fine fuel moisture and fire activity observed later in the day (*13*). Such noon-specific data are often absent from observational records and publicly available climate model outputs [e.g., from the Earth System Grid Federation (*57*)], prompting reliance on approximations that minimize trend distortion (*58*–*60*). On the other hand, the use of daily mean aggregated inputs has been discouraged for scenario estimation due to its deleterious effect on FWI trends and other FWI-derived indices often applied to characterize hazardous situations (*61*). Despite these findings, more recent studies suggest that daily mean inputs (e.g., daily mean temperature) may provide reasonable estimates of FWI95d, the yearly count of days above the local 95th percentile of daily FWI, yielding the least biased approximation among a set of input proxy versions (*43*).

In light of these findings, we calculate the FWI with daily means as a necessary simplification. In addition, to better assess the observational uncertainty associated with the underlying datasets, we used two state-of-the-art reanalyses, ERA5 and JRA55. We also tested whether removing regions with large noon versus daily discrepancies [as identified by Matteo *et al.* (*43*)] altered the results. For modeled data, we distinguished internal climate variability (from preindustrial control "piControl" runs) from externally forced changes (from historical plus SSP2-4.5 simulations). Combining these two forcing periods (HIST+245) facilitates comparisons between simulations and observations over the full 44-year window (1980–2023). All model outputs originated from the CMIP6.

We calculated the FWI using the fireDanger R package [v1.1.0; (*62*–*64*)]. To address the limitations posed by the absence of subdaily meteorological data in the climate models used here, we used daily approximations for calculating the FWI. Specifically, we used a combination of daily mean values for temperature, RH, wind speed, and 24-hour accumulated precipitation. This approach was chosen on the basis of prior findings (*43*), which identified daily mean values as the least biased alternative for approximating FWI trends calculated with noon-specific data (*27*). In addition, we accounted for potential biases by testing the results both with and without the inclusion of areas where these approximations do not preserve the noon-specific trends (see Fig. 3 and fig. S7). Following the methodology of (*9*), we calculated the annual number of days (FWI95d) on which the FWI exceeds the 95th percentile of all daily observations during the baseline period, computed separately for each grid cell. The baseline period covers 1980–2023 for both observations and HIST+245 simulations and the past 449 years for the control runs.

Reanalysis and CMIP6 climate simulations

We used the ERA5 reanalysis dataset (*25*), based on the model IFS Cy41r2 used in the European Centre for Medium Range Weather Forecasts operational medium-range forecasting system (~31 km), and the JRA55 reanalysis dataset (*26*), based on the Japan Meteorological Agency (JMA) global spectral model (~55 km), to derive daily mean values of the required input variables—2-m temperature, 2-m RH, 10-m wind speed, and 24-hour accumulated precipitation—as detailed in (*43*). The analysis period spans from 1980 to 2023. Although FWI was initially calculated for the full period of 1979–2023 for ERA5 and JRA55, data from 1979 were excluded to avoid spin-up biases due to initialization of fuel moisture codes (see the Supplementary Materials for more details on FWI calculation). While both ERA5 and JRA-55 technically provide data for years before 1979 (*26*, *35*), only from 1979 onward do they assimilate satellite observations. This marks a major improvement in the spatial and temporal coverage of assimilated data and reduces the risk of artificial discontinuities. Therefore, to ensure a consistent and homogeneous analysis, we start in 1980.

For our climate simulations, we used 10 models from CMIP6 (*23*) that provide the necessary daily mean input variables (tables S1 to S3). The models and runs included were selected on the basis of their availability in the Earth System Grid Federation (ESGF) infrastructure at the beginning of our analysis (early 2024), ensuring that

all required experiments (historical, SSP2-4.5, and piControl) and variables (daily tas, hurs, sfcWind, and pr) were accessible without relevant ESGF download issues. The study focuses on three types of numerical experiments:

1) Historical experiments (1979–2014): Simulate the influence of both human and natural external forcings on the climate system.

2) Future experiments based on the SSP2-4.5 pathway (2015–2023): Represent moderate changes in external forcings.

3) Preindustrial control simulations: Represent a climate with no changes in external forcings.

Following CMIP6 guidelines (*24*), we concatenated historical simulations with SSP2-4.5 simulations to create continuous datasets over the full observed FWI period, referring to these combined simulations as HIST+245. From 86 simulations across the 10 models (table S1), we calculated daily FWI values for the period 1980–2023, excluding the first year (1979) to mitigate spin-up effects.

The preindustrial control simulations have a maximum temporal coverage of 450 years among the models considered. To ensure consistency, we used the past 450 years of each model's control run, excluding the first year to avoid spin-up biases. This approach provided a total of 4490 (10 × 449) years of concatenated control run data for analysis. Climate simulations were accessed via the User Data Gateway of the Santander MetGroup (https://meteo.unican.es/udg-tap/home).

The subset of models selected spans a broad range of climate sensitivities, as represented by their Equilibrium Climate Sensitivity (ECS) values. Using ECS values from (*65*), our subset is representative of the broader CMIP6 ECS range:

1) Percentiles (all CMIP6 models): 10th = 2.52, median = 3.76, 90th = 5.34

2) Percentiles (models used in this study): 10th = 2.60, median = 3.73, 90th = 5.20

This selection process also highlights a critical limitation within CMIP6: Many models were excluded because one or more required variables or experiments were unavailable. This underscores the importance, particularly for CMIP7, of providing essential variables such as temperature, humidity, wind speed, and precipitation at daily (or ideally hourly) resolution across all core experiments (historical, SSP scenarios, and piControl) to facilitate comprehensive detection and attribution analyses.

Grid

To ensure consistency across datasets, all input variables were bilinearly remapped to a standardized 1° by 1° grid, as defined in the IPCC Sixth Assessment Report (*66*). This step may, in principle, reduce the consistency among variables when interpolated separately. However, such upscaling of the reanalysis data is necessary to enable fair comparisons between these data and climate models, which typically operate at coarser resolutions. Moreover, in a previous study (*43*), we specifically tested the impact of the remapping strategy on FWI trends: We compared two approaches—(i) computing FWI at 0.25° resolution and then remapping it to 1° and (ii) remapping the input variables to 1° before computing FWI—and found negligible differences between the resulting FWI trends. This confirms that the chosen approach does not introduce substantial artifacts for long-term trend analysis.

Subsequently, we masked areas with infrequent fire activity. Following the approach of (*60*), we applied a mask based on the European Space Agency Climate Change Initiative land cover dataset from 2016 (*67*). Grid cells with >80% bare areas, water, snow/ice, or sparse vegetation are excluded as areas with infrequent burning. The mask is available at (*68*).

Fingerprint analysis

Detection methods often require an estimate of the true but unknown climate change signal resulting from individual or combined forcings (*28*), commonly referred to as the fingerprint $F(x)$. Full methodological details can be found in (*29*).

The fingerprint can be defined in various ways. In our approach, we define $F(x)$ as the first EOF of the multimodel mean change in FWI95d from the HIST+245 simulations.

Let $S(i, j, x, t)$ represent the annual FWI95d at grid point x and time t, obtained from the ith realization of the jth model's HIST+245 simulation, where:

1) $i = 1, ..., N_r(j)$ (the number of realizations for the jth model).

2) $j = 1, ..., N_m$ (the total number of models used in fingerprint estimation).

3) $x = 1, ..., N_x$ (the total number of grid points).

4) $t = 1, ..., N_t$ (the number of years).

In this context:

1) N_r ranges from 1 to 40 ensemble members.

2) $N_m = 7$ models.

3) On the common 1° by 1° latitude/longitude grid, there are $N_x = 13{,}264$ unmasked land grid points.

4) $N_t = 44$ years.

We calculated the multimodel mean change $\langle\langle S(x,t)\rangle\rangle$ by first averaging ($\langle\rangle$) over the ensemble realizations for each model's HIST+245 simulations (where multiple realizations were available) and then averaging across all models. The double angular brackets denote these two averaging steps. Anomalies at each grid point x and time t were then defined relative to the local climatological annual mean. The fingerprint $F(x)$ is subsequently defined as the first EOF of these anomalies in $\langle\langle S(x,t)\rangle\rangle$.

To determine whether the pattern similarity between time-varying observations and $F(x)$ exhibits a statistically significant increase over time, we rely on control run estimates of internally generated variability. These control runs provide a baseline in which the fingerprint is absent except by chance. We derive variability estimates from control runs performed with multiple models, yielding a total of 4490 years of concatenated data. Anomalies are calculated relative to the climatological annual means over the full 449-year length of each model's control run. To avoid biases in S/N estimates, drift, defined as the linear trend over the full control simulation, is removed by approximating it as a least-squares linear trend and subtracting it at each grid point. This correction is consistently applied across the entire 449-year period of each model.

Observed temperature data for FWI95d are expressed as anomalies relative to climatological means over 1980–2023. These anomalies are projected onto the time-invariant fingerprint $F(x)$, as follows

$$z_o(t) = \sum_{x=1}^{N_x} 0(x,t)F(x), t = 1, \ \ldots, 44 \quad (1)$$

Here, $O(x, t)$ represents the observed annual mean or annual cycle amplitude data, while $F(x)$ denotes the fingerprint. This projection is equivalent to the spatially uncentered covariance between $O(x, t)$ and $F(x)$ at each year t. The resulting signal time series $Z_o(t)$ reflects the strength of the fingerprint in the observations. If observed temperature patterns increasingly resemble $F(x)$, $Z_o(t)$ will exhibit a positive trend over time.

To evaluate the significance of this trend, we replace $O(x, t)$ with the concatenated noise dataset $C(x, t)$, constructed from the outputs of model control simulations. The noise time series $N_c(t)$ is defined as

$$N_c(t) = \sum_{x=1}^{N_x} C(x,t)F(x), t = 1, \ldots, 3143 \quad (2)$$

We estimate S/N ratios by fitting least-squares linear trends of length L years to $Zo(t)$ and comparing these trends to the SD of overlapping L-year trends in $N_c(t)$. Signal detection occurs when the trend in $Z_o(t)$ consistently exceeds a specified significance level (e.g., 1%). This test is one-tailed, assuming a Gaussian distribution of trends in $N_c(t)$.

The start date for trend fitting is 1980, the first complete year of observational data. We use a minimum trend length of 10 years, making the first S/N ratio and earliest detection possible for 10-year trends ending in 1989.

Last, we emphasize that all model and observational temperature data used in the fingerprint analysis are appropriately area weighted. This weighting is achieved by multiplying the data by the square root of the cosine of the latitude at each grid node. However, for visual representation purposes in the figure's maps, the EOFs are displayed without weighting.

Supplementary Materials

This PDF file includes:

Supplementary Text
Figs. S1 to S7
Tables S1 to S3
References

REFERENCES

1. R. A. Bradstock, A biogeographic model of fire regimes in Australia: Current and future implications. *Glob. Ecol. Biogeogr.* **19**, 145–158 (2010).
2. D. M. J. S. Bowman, C. A. Kolden, J. T. Abatzoglou, F. H. Johnston, G. R. van der Werf, M. Flannigan, Vegetation fires in the Anthropocene. *Nat. Rev. Earth Environ.* **1**, 500–515 (2020).
3. J. G. Pausas, J. E. Keeley, Wildfires and global change. *Front. Ecol. Environ.* **19**, 387–395 (2021).
4. D. M. J. S. Bowman, G. J. Williamson, J. T. Abatzoglou, C. A. Kolden, M. A. Cochrane, A. M. S. Smith, Human exposure and sensitivity to globally extreme wildfire events. *Nat. Ecol. Evol.* **1**, 0058 (2017).
5. C. X. Cunningham, G. J. Williamson, D. M. J. S. Bowman, Increasing frequency and intensity of the most extreme wildfires on Earth. *Nat. Ecol. Evol.* **8**, 1420–1425 (2024).
6. M. W. Jones, D. I. Kelley, C. A. Burton, F. Di Giuseppe, M. L. F. Barbosa, E. Brambleby, A. J. Hartley, A. Lombardi, G. Mataveli, J. R. McNorton, F. R. Spuler, J. B. Wessel, J. T. Abatzoglou, L. O. Anderson, N. Andela, S. Archibald, D. Armenteras, E. Burke, R. Carmenta, E. Chuvieco, H. Clarke, S. H. Doerr, P. M. Fernandes, L. Giglio, D. S. Hamilton, S. Hantson, S. Harris, P. Jain, C. A. Kolden, T. Kurvits, S. Lampe, S. Meier, S. New, M. Parrington, M. M. G. Perron, Y. Qu, N. S. Ribeiro, B. H. Saharjo, J. San-Miguel-Ayanz, J. K. Shuman, V. Tanpipat, G. R. van der Werf, S. Veraverbeke, G. Xanthopoulos, State of Wildfires 2023–2024. *Earth Syst. Sci. Data* **16**, 3601–3685 (2024).
7. P. Jain, D. Castellanos-Acuna, S. C. P. Coogan, J. T. Abatzoglou, M. D. Flannigan, Observed increases in extreme fire weather driven by atmospheric humidity and temperature. *Nat. Clim. Change* **12**, 63–70 (2022).
8. W. M. Jolly, M. A. Cochrane, P. H. Freeborn, Z. A. Holden, T. J. Brown, G. J. Williamson, D. M. J. S. Bowman, Climate-induced variations in global wildfire danger from 1979 to 2013. *Nat. Commun.* **6**, 7537 (2015).
9. M. W. Jones, J. T. Abatzoglou, S. Veraverbeke, N. Andela, G. Lasslop, M. Forkel, A. J. P. Smith, C. Burton, R. A. Betts, G. R. van der Werf, S. Sitch, J. G. Canadell, C. Santín, C. Kolden, S. H. Doerr, C. Le Quéré, Global and regional trends and drivers of fire under climate change. *Rev. Geophys.* **60**, e2020RG000726 (2022).
10. D. Richardson, D. I. Kelley, F. Di Giuseppe, S. Remy, M. Parrington, Global increase in wildfire potential from compound fire weather and drought. *npj Clim. Atmos. Sci.* **5**, 23 (2022).
11. M. Á. Torres-Vázquez, F. Di Giuseppe, A. Moreno-Torreira, A. Gincheva, S. Jerez, M. Turco, Large increase in extreme fire weather synchronicity over Europe. *Environ. Res. Lett.* **20**, 034052 (2025).
12. Z. Liu, J. M. Eden, B. Dieppois, M. Blackett, A global view of observed changes in fire weather extremes: Uncertainties and attribution to climate change. *Clim. Change* **173**, 14 (2022).
13. C. E. van Wagner, "Development and Structure of the Canadian Forest Fire Weather Index System" (Canadian Forestry Service, technical report 35, 1987); https://ostrnrcan-dostrncan.canada.ca/handle/1845/228434.
14. Y. Zhuang, R. Fu, B. D. Santer, R. E. Dickinson, A. Hall, Quantifying contributions of natural variability and anthropogenic forcings on increased fire weather risk over the western United States. *Proc. Natl. Acad. Sci. U.S.A.* **118**, e2111875118 (2021).
15. F. Justino, D. H. Bromwich, V. Schumacher, A. DaSilva, S.-H. Wang, Arctic Oscillation and Pacific–North American pattern dominated-modulation of fire danger and wildfire occurrence. *npj Clim. Atmos. Sci.* **5**, 52 (2022).
16. G. Liu, J. Li, T. Ying, Atlantic Multidecadal Oscillation modulates the relationship between El Niño–Southern Oscillation and fire weather in Australia. *Atmos. Chem. Phys.* **23**, 9217–9228 (2023).
17. M. Rodrigues, D. Peña-Ángulo, A. Russo, M. Zúñiga-Antón, A. Cardil, Do climate teleconnections modulate wildfire-prone conditions over the Iberian Peninsula? *Environ. Res. Lett.* **16**, 044050 (2021).
18. H. Zheng, L. Xue, K. Ding, S. Lou, Z. Wang, A. Ding, X. Huang, ENSO-related fire weather changes in southeast and equatorial Asia: A quantitative evaluation using Fire Weather Index. *J. Geophys. Res. Atmos.* **128**, e2023JD039688 (2023).
19. A. Barik, S. Baidya Roy, Climate change strongly affects future fire weather danger in Indian forests. *Commun. Earth Environ.* **4**, 452 (2023).
20. A. Liné, C. Cassou, R. Msadek, S. Parey, Modulation of Northern Europe near-term anthropogenic warming and wettening assessed through internal variability storylines. *npj Clim. Atmos. Sci.* **7**, 272 (2024).
21. J. L. Martel, A. Mailhot, F. Brissette, D. Caya, Role of natural climate variability in the detection of anthropogenic climate change signal for mean and extreme precipitation at local and regional scales. *J. Clim.* **31**, 4241–4263 (2018).
22. J. Miller, A. Böhnisch, R. Ludwig, M. I. Brunner, Climate change impacts on regional fire weather in heterogeneous landscapes of central Europe. *Nat. Hazards Earth Syst. Sci.* **24**, 411–428 (2024).
23. V. Eyring, S. Bony, G. A. Meehl, C. A. Senior, B. Stevens, R. J. Stouffer, K. E. Taylor, Overview of the Coupled Model Intercomparison Project Phase 6 (CMIP6) experimental design and organization. *Geosci. Model Dev.* **9**, 1937–1958 (2016).
24. N. P. Gillett, H. Shiogama, B. Funke, G. Hegerl, R. Knutti, K. Matthes, B. D. Santer, D. Stone, C. Tebaldi, The Detection and Attribution Model Intercomparison Project (DAMIP v1.0) contribution to CMIP6. *Geosci. Model Dev.* **9**, 3685–3697 (2016).
25. H. Hersbach, B. Bell, P. Berrisford, S. Hirahara, A. Horányi, J. Muñoz-Sabater, J. Nicolas, C. Peubey, R. Radu, D. Schepers, A. Simmons, C. Soci, S. Abdalla, X. Abellan, G. Balsamo, P. Bechtold, G. Biavati, J. Bidlot, M. Bonavita, G. De Chiara, P. Dahlgren, D. Dee, M. Diamantakis, R. Dragani, J. Flemming, R. Forbes, M. Fuentes, A. Geer, L. Haimberger, S. Healy, R. J. Hogan, E. Hólm, M. Janisková, C. Keeley, P. Laloyaux, P. Lopez, C. Lupu, G. Radnoti, P. de Rosnay, I. Rozum, F. Vamborg, S. Villaume, J.-N. Thépaut, The ERA5 global reanalysis. *Q. J. Roy. Meteorol. Soc.* **146**, 1999–2049 (2020).
26. S. Kobayashi, Y. Ota, Y. Harada, A. Ebita, M. Moriya, H. Onoda, K. Onogi, H. Kamahori, C. Kobayashi, H. Endo, K. Miyaoka, K. Takahashi, The JRA-55 reanalysis: General specifications and basic characteristics. *J. Meteor. Soc. Japan* **93**, 5–48 (2015).
27. C. Vitolo, F. Di Giuseppe, C. Barnard, R. Coughlan, J. San-Miguel-Ayanz, G. Libertá, B. Krzeminski, ERA5-based global meteorological wildfire danger maps. *Sci. Data* **7**, 216 (2020).
28. K. Hasselmann, "On the signal-to-noise problem in atmospheric response studies," in *Meteorology Over the Tropical Oceans*, D. B. Shaw Ed. (Royal Meteorological Society, 1979), pp. 251–259.
29. B. D. Santer, J. F. Painter, C. A. Mears, C. Doutriaux, P. Caldwell, J. M. Arblaster, T. M. L. Wigley, S. Solomon, P. J. Durack, J. G. Fyfe, N. P. Gillett, G. A. Meehl, R. W. Portmann, B. D. Santer, C.-Z. Zou, Identifying human influences on atmospheric temperature. *Proc. Natl. Acad. Sci. U.S.A.* **110**, 26–33 (2013).
30. B. D. Santer, S. Po-Chedley, M. D. Zelinka, I. Cvijanovic, C. Bonfils, P. J. Durack, Q. Fu, J. M. Kiehl, C. Mears, J. F. Painter, G. Pallotta, S. Solomon, F. J. Wentz, C.-Z. Zou, Human influence on the seasonal cycle of tropospheric temperature. *Science* **361**, eaas8806 (2018).
31. B. D. Santer, S. Po-Chedley, L. Zhao, C.-Z. Zou, Q. Fu, S. Solomon, K. E. Taylor, Exceptional stratospheric contribution to human fingerprints on atmospheric temperature. *Proc. Natl. Acad. Sci. U.S.A.* **120**, e2300758120 (2023).
32. C. J. W. Bonfils, B. D. Santer, J. C. Fyfe, K. Marvel, T. J. Phillips, S. R. H. Zimmerman, Human influence on joint changes in temperature, rainfall and continental aridity. *Nat. Clim. Change* **10**, 726–731 (2020).
33. K. Marvel, B. I. Cook, C. J. W. Bonfils, P. J. Durack, J. E. Smerdon, A. P. Williams, Twentieth-century hydroclimate changes consistent with human influence. *Nature* **569**, 59–65 (2019).

34. S. El Garroussi, F. Di Giuseppe, C. Barnard, F. Wetterhall, Europe faces up to tenfold increase in extreme fires in a warming climate. *npj Clim. Atmos. Sci.* **7**, 30 (2024).
35. C. Soci, H. Hersbach, A. J. Simmons, P. Poli, B. Bell, P. Berrisford, A. Horányi, J. Muñoz-Sabater, J. Nicolas, R. Radu, D. Schepers, S. Villaume, L. Haimberger, J. Woollen, C. Buontempo, J.-N. Thépaut, The ERA5 global reanalysis from 1940 to 2022. *Q. J. Roy. Meteorol. Soc.* **150**, 4014–4048 (2024).
36. K. E. Trenberth, J. T. Fasullo, J. Mackaro, Atmospheric moisture transports from ocean to land and global energy flows in reanalyses. *J. Clim.* **24**, 4907–4924 (2011).
37. U. Pfeifroth, R. Mueller, B. Ahrens, Evaluation of satellite-based and reanalysis precipitation data in the tropical Pacific. *J. Appl. Meteorol. Climatol.* **52**, 634–644 (2013).
38. D. A. Lavers, A. Simmons, F. Vamborg, M. J. Rodwell, An evaluation of ERA5 precipitation for climate monitoring. *Q. J. Roy. Meteorol. Soc.* **148**, 3152–3165 (2022).
39. I. R. Simpson, K. A. McKinnon, D. Kennedy, D. M. Lawrence, F. Lehner, R. Seager, Observed humidity trends in dry regions contradict climate models. *Proc. Natl. Acad. Sci. U.S.A.* **121**, e2302480120 (2024).
40. C. Zhou, M. D. Zelinka, S. A. Klein, Impact of decadal cloud variations on the Earth's energy budget. *Nat. Geosci.* **9**, 871–874 (2016).
41. K. Marvel, R. Pincus, G. A. Schmidt, R. L. Miller, Internal variability and disequilibrium confound estimates of climate sensitivity from observations. *Geophys. Res. Lett.* **45**, 1595–1601 (2018).
42. T. Kitzberger, P. M. Brown, E. K. Heyerdahl, T. W. Swetnam, T. T. Veblen, Contingent Pacific–Atlantic Ocean influence on multicentury wildfire synchrony over western North America. *Proc. Natl. Acad. Sci. U.S.A.* **104**, 543–548 (2007).
43. A. Matteo, G. Garnés-Morales, A. Moreno, A. F. S. Ribeiro, C. Azorin-Molina, J. Bedia, F. Di Giuseppe, R. J. H. Dunn, S. Herrera, A. Provenzale, Y. Quilcaille, M. Á. Torres-Vázquez, M. Turco, Challenges in assessing Fire Weather changes in a warming climate. *npj Clim. Atmos. Sci.* **8**, 284 (2025).
44. P. E. Higuera, J. T. Abatzoglou, Record-setting climate enabled the extraordinary 2020 fire season in the western United States. *Glob. Change Biol.* **27**, 1–2 (2021).
45. D. I. Kelley, C. Burton, C. Huntingford, M. A. J. Brown, R. Whitley, N. Dong, Low meteorological influence found in 2019 Amazonia fires. *Biogeosciences* **18**, 787–804 (2021).
46. M. C. Kirchmeier-Young, E. Malinina, Q. E. Barber, K. Garcia Perdomo, S. R. Curasi, Y. Liang, P. Jain, N. P. Gillett, M.-A. Parisien, A. J. Cannon, A. R. Lima, V. K. Arora, Y. Boulanger, J. R. Melton, L. Van Vliet, X. Zhang, Human driven climate change increased the likelihood of the 2023 record area burned in Canada. *npj Clim. Atmos. Sci.* **7**, 316 (2024).
47. M. Turco, J. T. Abatzoglou, S. Herrera, Y. Zhuang, S. Jerez, D. D. Lucas, A. AghaKouchak, I. Cvijanovic, Anthropogenic climate change impacts exacerbate summer forest fires in California. *Proc. Natl. Acad. Sci. U.S.A.* **120**, e2213815120 (2023).
48. P. A. Arias, N. Bellouin, E. Coppola, R. G. Jones, G. Krinner, J. Marotzke, V. Naik, M. D. Palmer, G.-K. Plattner, J. Rogelj, M. Rojas, J. Sillmann, T. Storelvmo, P. W. Thorne, B. Trewin, K. Achuta Rao, B. Adhikary, R. P. Allan, K. Armour, G. Bala, R. Barimalala, S. Berger, J. G. Canadell, C. Cassou, A. Cherchi, W. Collins, W. D. Collins, S. L. Connors, S. Corti, F. Cruz, F. J. Dentener, C. Dereczynski, A. Di Luca, A. Diongue Niang, F. J. Doblas-Reyes, A. Dosio, H. Douville, F. Engelbrecht, V. Eyring, E. M. Fischer, P. Forster, B. Fox-Kemper, J. S. Fuglestvedt, J. C. Fyfe, N. P. Gillett, L. Goldfarb, I. Gorodetskaya, J. M. Gutiérrez, R. Hamdi, E. Hawkins, H. T. Hewitt, P. Hope, A. S. Islam, C. Jones, D. S. Kaufman, R. E. Kopp, Y. Kosaka, J. Kossin, S. Krakovska, J.-Y. Lee, J. Li, T. Mauritsen, T. K. Maycock, M. Meinshausen, S.-K. Min, P. M. S. Monteiro, T. Ngo-Duc, F. Otto, I. Pinto, A. Pirani, K. Raghavan, R. Ranasinghe, A. C. Ruane, L. Ruiz, J.-B. Sallée, B. H. Samset, S. Sathyendranath, S. I. Seneviratne, A. A. Sörensson, S. Szopa, I. Takayabu, A.-M. Tréguier, B. van den Hurk, R. Vautard, K. von Schuckmann, S. Zaehle, X. Zhang, K. Zickfeld, "Technical summary," in *Climate Change 2021: The Physical Science Basis. Contribution of Working Group I to the Sixth Assessment Report of the Intergovernmental Panel on Climate Change*, V. Masson-Delmotte, P. Zhai, A. Pirani, S. L. Connors, C. Péan, S. Berger, N. Caud, Y. Chen, L. Goldfarb, M. I. Gomis, M. Huang, K. Leitzell, E. Lonnoy, J. B. R. Matthews, T. K. Maycock, T. Waterfield, O. Yelekçi, R. Yu, B. Zhou, Eds. (Cambridge Univ. Press, 2021), pp. 33–144.
49. V. Chandrashekhar, A global warming 'hole' where you'd least expect it. *Science* **388**, 136 (2025).
50. W. J. de Groot, M. D. Flannigan, "Climate change and early warning systems for wildland fire," in *Reducing Disaster: Early Warning Systems for Climate Change*, Z. Zommers, A. Singh, Eds. (Springer, 2014), pp. 127–151.
51. S. W. Taylor, M. E. Alexander, Science, technology, and human factors in fire danger rating: The Canadian experience. *Int. J. Wildland Fire* **15**, 121–135 (2006).
52. A. Gincheva, J. G. Pausas, M. Á. Torres-Vázquez, J. Bedia, S. M. Vicente-Serrano, J. T. Abatzoglou, J. A. Sánchez-Espigares, E. Chuvieco, S. Jerez, A. Provenzale, R. M. Trigo, M. Turco, The interannual variability of global burned area is mostly explained by climatic Drivers. *Earth's Future* **12**, e2023EF004334 (2024).
53. E. Kalnay, M. Kanamitsu, R. Kistler, W. Collins, D. Deaven, L. Gandin, M. Iredell, S. Saha, G. White, J. Woollen, Y. Zhu, M. Chelliah, W. Ebisuzaki, W. Higgins, J. Janowiak, K. C. Mo, C. Ropelewski, J. Wang, A. Leetmaa, R. Reynolds, R. Jenne, D. Joseph, The NCEP/NCAR 40-Year Reanalysis Project. *Bull. Am. Meteorol. Soc.* **77**, 437–472 (1996).
54. J. Bedia, S. Herrera, J. M. Gutiérrez, G. Zavala, I. R. Urbieta, J. M. Moreno, Sensitivity of fire weather index to different reanalysis products in the Iberian Peninsula. *Nat. Hazards Earth Syst. Sci.* **12**, 699–708 (2012).
55. R. Buizza, "Ensemble forecasting and the need for calibration," in *Statistical Postprocessing of Ensemble Forecasts,* L. J. Some, S. Vannitsem, D. S. Wilks, J. W. Messner, Eds. (Elsevier, 2018), pp. 15–48.
56. W. S. Parker, Reanalyses and observations: What's the difference? *Bull. Am. Meteorol. Soc.* **97**, 1565–1572 (2016).
57. L. Cinquini, D. Crichton, C. Mattmann, J. Harney, G. Shipman, F. Wang, R. Ananthakrishnan, N. Miller, S. Denvil, M. Morgan, Z. Pobre, G. M. Bell, B. Drach, D. Williams, P. Kershaw, S. Pascoe, E. Gonzalez, S. Fiore, R. Schweitzer, The Earth System Grid Federation: An open infrastructure for access to distributed geospatial data. *Future Gener. Comput. Syst.* **36**, 400–417 (2014).
58. J. T. Abatzoglou, A. P. Williams, R. Barbero, Global emergence of anthropogenic climate change in fire weather indices. *Geophys. Res. Lett.* **46**, 326–336 (2019).
59. J. Bedia, S. Herrera, A. Camia, J. M. Moreno, J. M. Gutiérrez, Forest Fire Danger Projections in the Mediterranean using ENSEMBLES Regional Climate Change Scenarios. *Clim. Change* **122**, 185–199 (2014).
60. Y. Quilcaille, F. Batibeniz, A. F. Ribeiro, R. S. Padrón, S. I. Seneviratne, Fire Weather Index data under historical and shared socioeconomic pathway projections in the 6th phase of the Coupled Model Intercomparison Project from 1850 to 2100. *Earth Syst. Sci. Data* **15**, 2153–2177 (2023).
61. S. Herrera, J. Bedia, J. M. Gutiérrez, J. Fernández, J. M. Moreno, On the projection of future fire danger conditions with various instantaneous/mean-daily data sources. *Clim. Change* **118**, 827–840 (2013).
62. M. Iturbide, J. Bedia, S. Herrera, J. Baño-Medina, J. Fernández, M. D. Frías, R. Manzanas, D. San-Martín, E. Cimadevilla, A. S. Cofiño, J. M. Gutiérrez, The R-based climate4R open framework for reproducible climate data access and post-processing. *Environ. Model. Softw.* **111**, 42–54 (2019).
63. C. E. Van Wagner, T. L. Pickett, Equations and FORTRAN program for the Canadian Forest Fire Weather Index System (Forestry Technical Report 33, Canadian Forestry Service, Petawawa National Forestry Institute, Chalk River, Ontario, 1985), p. 18.
64. B. D. Lawson, O. B. Armitage, Weather Guide for the Canadian Forest Fire Danger Rating System. Northern Forestry Centre Guidebook (2008). Edmonton, Alberta. https://ostrnrcan-dostrncan.canada.ca/handle/1845/219568.
65. Z. Hausfather, K. Marvel, G. A. Schmidt, J. W. Nielsen-Gammon, M. Zelinka, Climate simulations: Recognize the 'hot model' problem. *Nature* **605**, 26–29 (2022).
66. M. Iturbide, J. Fernández, J. M. Gutiérrez, A. Pirani, D. Huard, A. Al Khourdajie, J. Baño-Medina, J. Bedia, A. Casanueva, E. Cimadevilla, A. S. Cofiño, M. De Felice, J. Díez-Sierra, M. García-Díez, J. Goldie, D. A. Herrera, S. Herrera, R. Manzanas, J. Milovac, A. Radhakrishnan, D. San-Martín, A. Spinuso, K. M. Thyng, C. Trenham, Ö. Yelekçi, Implementation of FAIR principles in the IPCC: The WGI AR6 Atlas repository. *Sci. Data* **9**, 629 (2022).
67. P. Defourny, ESA Land Cover Climate Change Initiative (Land_Cover_cci): Land Cover Maps v2.0.7. Centre for Environmental Data Analysis (2017); https://esa-landcover-cci.org/.
68. M. Turco, A. Moreno-Torreira, Global Fire Danger Masks at 1° Resolution: Delineating Infrequent Fires and Trend Inconsistencies [Data set]. Zenodo (2025); https://doi.org/10.5281/zenodo.14964973.

Acknowledgments: We thank B. D. Santer for insightful comments. We wish to acknowledge the reviewers for detailed and helpful comments on the original manuscript. **Funding:** This work was supported by the "Climate and Wildfire Interface Study for Europe (CHASE)" project under the 6th Seed Funding Call by the European University for Well-Being (EUniWell). M.T. acknowledges funding by the Spanish Ministry of Science, Innovation and Universities through the Ramón y Cajal Grant (reference RYC2019-027115-I) and the project ONFIRE (grant PID2021-123193OB-I00), funded by MCIN/AEI/10.13039/501100011033 and by "ERDF A way of making Europe." A.P. acknowledges support from the H2020 EU project "FirEUrisk" (grant no. 101003890). **Author contributions:** Conceptualization: M.T. and J.B. Funding acquisition: M.T. Methodology: M.T., A.M., and J.B. Investigation: M.T. and J.B. Resources: M.T., F.D.G., and J.B. Data curation: M.T., G.G.-M., F.D.G., and J.B. Software: M.T., J.B., and S.H. Formal analysis: A.M. and M.T. Validation: M.T. Supervision: M.T. Project administration: M.T. Visualization: M.T. Writing—original draft: M.T., A.M., A.P., J.B., and M.V. Writing—review and editing: All authors. **Competing interests:** The authors declare that they have no competing interests. **Data, code, and materials availability:** All data and code needed to evaluate and reproduce the results in the paper are present in the paper and/or the Supplementary Materials and are publicly available. The complete analysis code is publicly available at https://zenodo.org/records/17564195 and https://github.com/marcoturco/FWI_ATTRIBUTION. This study did not generate new materials.

Submitted 4 April 2025
Accepted 26 January 2026
Published 11 March 2026
10.1126/sciadv.adx9845

Science Advances

The emerging human fingerprint on global extreme fire weather

Marco Turco, Alberto Moreno, Ginés Garnés-Morales, Miguel Ángel Torres-Vázquez, Francesca Di Giuseppe, Joaquín Bedia, Sixto Herrera, Antonello Provenzale, and John T. Abatzoglou

Sci. Adv. **12** (11), eadx9845. DOI: 10.1126/sciadv.adx9845